Langmuir

Article

pubs.acs.org/Langmuir

Photoelectrochemical Properties of Nanomultiple $CaFe_2O_4/ZnFe_2O_4$ *pn* Junction Photoelectrodes

Junyu Cao,[†] Juanjuan Xing,[‡] Yuanjian Zhang,[§,⊥] Hua Tong,[∥] Yingpu Bi,[†,#] Tetsuya Kako,[†] Masaki Takeguchi,[‡] and Jinhua Ye*[,†,§,∥]

[†]Environmental Remediation Materials Unit, Catalytic Materials Group, [‡]Transmission Electron Microscopy Station, and [§]International Center for Materials Nanoarchitectonics (WPI-MANA), National Institute for Materials Science (NIMS), Tsukuba, Ibaraki, Japan

[∥]TU-NIMS Joint Research Center, School of Materials Science and Engineering, Tianjin University, 92 Weijin Road, Nankai District, Tianjin, PR China

Supporting Information

ABSTRACT: Nanomultiple $CaFe_2O_4/ZnFe_2O_4$ *pn* junctions are prepared by a pulsed laser deposition method to explore their photoelectrochemical properties as the photoelectrodes. It is demonstrated that the multiple-*pn*-junction structure is favorable to enhancing the photocurrent density and the onset potential of the photoelectrode. Furthermore, the 20-junction photoelectrode-based PEC cell yields a high open circuit photovoltage of up to 0.97 V, which is much higher than that for a single *pn* junction photoelectrode PEC cell that yields an open circuit photovoltage of 0.13 V. A multiple-junction band structure model is assumed to describe the behavior of the $CaFe_2O_4/ZnFe_2O_4$ multiple-junction photoelectrodes. It is suggested that the open circuit photovoltage is dominated by the number of *pn* junctions in a multiple-junction photoelectrode and the carrier transfer inside the photoelectrode is improved by narrowing the single-layer thickness. These findings provide a new approach to designing the multiple-junction structure to improve the PEC properties of the photoelectrodes.

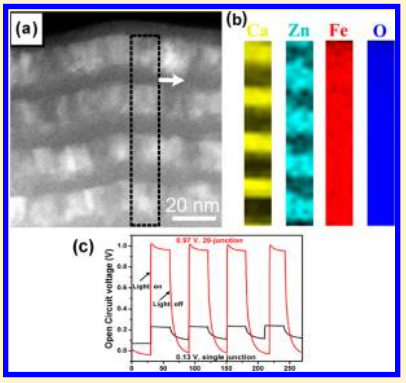

INTRODUCTION

Since Fujishima and Honda discovered water photolysis on the TiO_2 photoelectrode, hydrogen production through a photoelectrochemcial (PEC) approach has emerged as one of the most promising technologies because it represents an easy way to convert solar energy into chemical energy.[1] In a PEC cell, the photoelectrode is the most important part; it harvests incident light, generates electron−hole pairs, and performs PEC reactions on the surface.[2,3] Over the past decades, significant progress has been made in the development of photoelectrodes with various configurations and materials.[4−26] Among them, the multilayer photoelectrodes have attracted a lot of attention, owing to the advantages of enhancing the light utilization[23,24] or providing a photovoltage to assist PEC water splitting.[25,26] In multilayer photoelectrodes, a semiconductor *pn* junction usually functions as a photovoltaic cell to provide a photovoltage.[25,26] Another advantage of separating the electron and hole resulting from the depletion region of *pn* junction has attracted little attention. In the case of a single-layer semiconductor photoelectrode, the depletion region, which efficiently separates the electron and hole, exists only in a small region (tens of nanometers) at the electrode−electrolyte interface.[27] Most of the area inside the photoelectrode belongs to the neutral region, which does not possess the ability to separate the electron and hole. By fabricating nanomultiple *pn* junction photoelectrodes, numerous depletion regions could be created even inside the photoelectrode. It is worth expecting that the nanomultiple *pn* junction structure could enhance the electron−hole separation and the carrier transfer, thus resulting in the improvement of the PEC properties.

However, there are two issues that need to be addressed pertaining to the multiple-junction thin film being utilized as a photoelectrode. (1) Does the carrier transfer driven by the *pn* junctions favor the PEC performance of the *pn* junction photoelectrodes? As the photoelectrode, the *p* semiconductor acts as a cathode for the PEC reduction reaction (*p*-cathode) and the *n* semiconductor acts as the anode for PEC oxidization reaction (*n*-anode) because of the effect of the depletion region at the electrode−electrolyte interface.[1,4] Nevertheless, a conventional *pn* junction could drive only the photogenerated electron transfer from the *p* side to the *n* side under light irradiation (*n*-cathode).[28] This electron transfer does not favor the application of *pn* junction as the photoelectrode. (2) Can the carrier transfer continuously in multiple-junction thin films? In the multiple-junction thin films, there are two kinds of space charge fields with opposite electronic field directions existing. An important question is whether the carrier can be transferred through these opposite space charge fields. It should be noticed

Received: November 5, 2012
Revised: February 7, 2013
Published: February 8, 2013

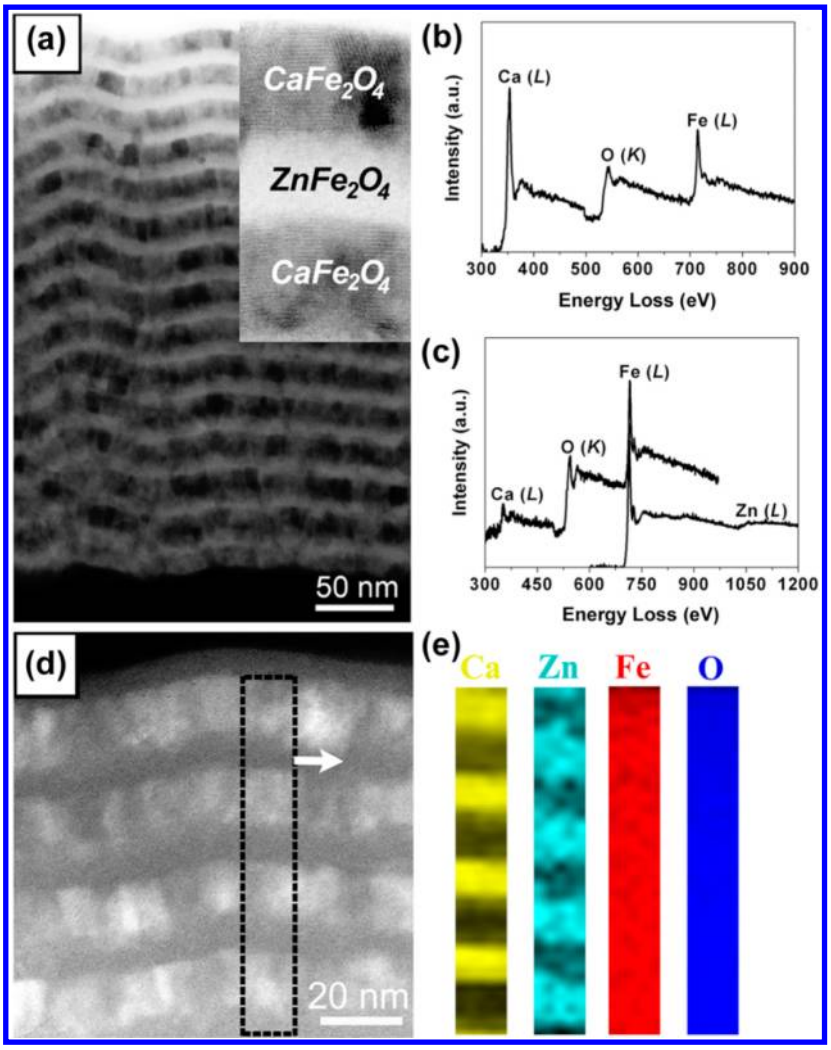

Figure 1. (a) Bright-field TEM image of a cross-sectional view of an alternately multilayered $CaFe_2O_4/ZnFe_2O_4$ film; each $CaFe_2O_4$ and $ZnFe_2O_4$ contains 15 layers with single-layer thicknesses of 15 and 10 nm, respectively. The inset shows an HRTEM image of the $CaFe_2O_4/ZnFe_2O_4$ alternate structure. (b) EELS spectra tested on a selective $CaFe_2O_4$ layer with an energy loss range from 300 to 970 eV. (c) EELS spectra tested on a selective $ZnFe_2O_4$ layer by two energy loss ranges: one is from 300 to 970 eV, and the other is from 600 to 1270 eV. (d) Dark-field TEM image of the $CaFe_2O_4/ZnFe_2O_4$ alternate structure, where spectrum imaging was carried out on a selective region for composition analysis. (e) Elemental maps of Ca, Zn, Fe, and O.

that, as the photoelectrodes, the multiple-junction photoelectrodes are immersed in the electrolyte and an additional depletion region exists at the electrode−electrolyte interface. This unique depletion region at the electrode−electrolyte interface is supposed to greatly change the performance of the multiple-junction thin films as a photoelectrode.

Here, we reported the fabrication of nanomultiple $CaFe_2O_4/ZnFe_2O_4$ *pn* junction photoelectrodes by a pulsed laser deposition (PLD) method. The PEC properties of the multiple $CaFe_2O_4/ZnFe_2O_4$ *pn* junction photoelectrodes were discussed in detail. It was found that the multiple-junction structure could significantly promote the PEC properties of the photoelectrodes, including the photocurrent density and the onset potential. On the basis of the experiment evidence, a multiple-junction band structure model was assumed to describe all of the behavior of the multiple $CaFe_2O_4/ZnFe_2O_4$ *pn* junction photoelectrodes.

■ EXPERIMENTAL SECTION

The thin films were prepared by the pulsed laser deposition (PLD) method using $CaFe_2O_4$ and $ZnFe_2O_4$ pellets as the targets and fluorine-doped tin oxide (FTO) as the substrate. The targets and FTO glass were set on the PLD machine (ST-PLD; Pascal Co., Japan), and the distance between the targets and FTO glass was set to be 5 cm. After that, the film-preparation chamber of the PLD machine was evacuated to 0.001 Pa, and then pure O_2 was introduced into the chamber until the pressure became 4 Pa. After the FTO glass was heated to 550 °C, the target was irradiated with a Nd:YAG laser at a wavelength of 355 nm. The repetition rate and the energy of the laser pulse length were 10 Hz and 62 mJ per pulse, respectively. After PLD deposition, the temperature was maintained for 1 h in the presence of O_2 (9.6×10^4 Pa) for postheat treatment of the samples.

The multilayer *p*-$CaFe_2O_4$/*n*-$ZnFe_2O_4$ junction electrodes with a single-layer thickness of 10−15 nm were prepared via the following steps: (I) depositing a $ZnFe_2O_4$ layer for 2.5 min and (II) depositing a $CaFe_2O_4$ layer on a prepared $ZnFe_2O_4$ layer for another 2.5 min. The processes (I and II) were repeated many times (10, 15, 20, and 25).

A field-emission scanning electron microscope (JSM-6701F, JEOL) and a transmission electron microscope (TEM, JEOL Co.) were used to characterize the samples. The cross-sectional TEM sample was prepared by Ga^+ focused ion beam (FIB) milling performed on a JEOL-9310 machine with a lift-out technique. The sample was milled to a thickness of less than 50 nm to make sure of the beam permeation. The microstructure was observed with a JEOL 300 keV

dx.doi.org/10.1021/la304377z | *Langmuir* 2013, 29, 3116−3124

field-emission TEM (JEM-3000F) and a JEOL Cs-corrected dedicated scanning TEM (JEM-2500SES) equipped with a Gatan 766 EELS spectrometer (Enfina 1000).

PEC properties of as-prepared thin films were characterized with an electrochemical station (ALS/CH model 650A) using three-electrode and two-electrode configurations. Platinum and Ag/AgCl were used as the counter electrode and reference electrode, respectively. In the photoelectrochemical measurement, the as-prepared electrodes were illuminated by light from the side of the electrolyte/film interface in aqueous Na_2SO_4 solution (0.1 M) through a quartz window. A 500 W xenon lamp (Optical Module X, USHIO, Japan) was utilized as the light source.

RESULTS AND DISCUSSION

p-$CaFe_2O_4$/*n*-$ZnFe_2O_4$ were adopted to explore the PEC properties of the multiple-junction thin films. $CaFe_2O_4$ and $ZnFe_2O_4$, which possess a favorable chemical stability in the aqueous solution, are naturally formed *p*-type and *n*-type oxide semiconductors, respectively. *n*-$ZnFe_2O_4$ shows a much more negative Fermi level (0.3 V versus Normal Hydrogen Electrode (NHE)) in comparison to *p*-$CaFe_2O_4$ (1.0 V vs NHE).[29−31] Therefore, it is reasonable to fabricate the *pn* heterojunction using $CaFe_2O_4$ and $ZnFe_2O_4$. Furthermore, as the photoelectrodes for PEC water splitting, $CaFe_2O_4$ and $ZnFe_2O_4$ possess identical narrow band gaps of 1.9 eV, which result in abundant visible light harvesting.[29−31] In addition, the conduction band edge of $CaFe_2O_4$ is located at −0.6 V versus NHE and the valence band edge of $ZnFe_2O_4$ is at +2.0 V versus NHE.[29−31] It is feasible to use a $CaFe_2O_4$/$ZnFe_2O_4$ *pn* junction for splitting water (H_2 reduction at 0 V vs NHE and O_2 oxidization at 1.23 V vs NHE).

The PLD method was utilized to prepare the multiple $CaFe_2O_4$/$ZnFe_2O_4$ *pn*-junction thin films. By changing the laser irradiation targets ($CaFe_2O_4$ and $ZnFe_2O_4$ pellets) back and forth, the $CaFe_2O_4$/ $ZnFe_2O_4$ multilayer was prepared simply on a fluorine-doped tin oxide (FTO) substrate. Meanwhile, by controlling the laser irradiation time on a target, the thickness of each layer was adjusted accurately. Here, it should be noticed that all the $CaFe_2O_4$/$ZnFe_2O_4$ multiple-junction thin films [FTO/$(ZnFe_2O_4/CaFe_2O_4)_x$] were composed by the direct tandem connection of the $CaFe_2O_4$/$ZnFe_2O_4$ junctions. Figure 1a presents the transmission electron microscope (TEM) image of a 15-junction photoelectrode [FTO/$(ZnFe_2O_4/CaFe_2O_4)_{15}$] with a single-layer thickness of about 10−15 nm. The bright-field TEM image of cross-section viewing (Figure 1a) displays the layer structure clearly because of the notable contrast resulting from the composition difference between neighboring $CaFe_2O_4$ and $ZnFe_2O_4$ layers. The compositions of multiple layers are further investigated by using electron energy loss spectroscopy (EELS) analysis (Figure 1b,c). The EELS spectra confirm the composition of both $CaFe_2O_4$ and $ZnFe_2O_4$ layers. Moreover, elemental maps (Figure 1d,e) indicate that the Fe and O elements spread evenly throughout all layers but Zn and Ca are distributed only in respective layers with apparent boundaries. These results provide solid evidence for the $CaFe_2O_4$/$ZnFe_2O_4$ multilayer structure.

The PEC properties of this 15-junction photoelectrode [FTO/$(ZnFe_2O_4/CaFe_2O_4)_{15}$] are measured in a 0.1 M Na_2SO_4 aqueous solution using a three-electrode configuration with Pt and Ag/AgCl electrodes as the counter electrode and reference electrode, respectively. In the current density versus potential (*J*−*V*) graph, a photocathodic current density is observed (red line, Figure 2) when the applied potential is more negative than 0.98 V versus Ag/AgCl. This result

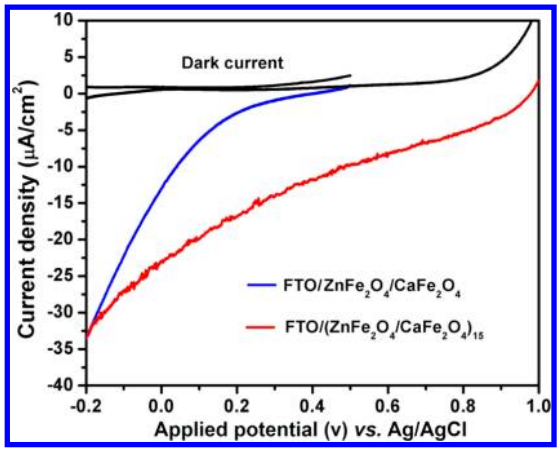

Figure 2. Current density vs potential (*J*−*V*) curves of the 15-junction photoelectrode (red line) and single $CaFe_2O_4$/$ZnFe_2O_4$ photoelectrode with the same thickness (blue line).

indicates that the 15-junction photoelectrode acts as the cathode for the PEC reduction reaction. Compared to the single-layer $CaFe_2O_4$ photocathode (the same thickness with this 15-junction photoelectrode), the 15-junction photoelectrode exhibits a much larger photocurrent density (−16.87 $\mu A/cm^2$ at 0.2 V vs Ag/AgCl) and a much more positive onset potential (0.98 V vs Ag/AgCl). These results show that the multiple-junction thin film has a significant enhancement effect on the PEC properties, including the photocurrent density and the onset potential. These results also imply that the multiple-junction structure should be favorable for improving the performance of the photoelectrode.

To clarify the mechanism of the multiple-junction photoelectrodes throughout, we start from studying the PEC properties of the thin films, which are the basic compositions of the $CaFe_2O_4$/$ZnFe_2O_4$ multiple junction (such as single-layer $CaFe_2O_4$, single-layer $ZnFe_2O_4$, and single $CaFe_2O_4$/ $ZnFe_2O_4$ *pn* junction thin films). All of these samples were fabricated by the PLD method on FTO substrates. The compositions of as-prepared $CaFe_2O_4$ and $ZnFe_2O_4$ single-layer thin films were successfully confirmed by using Raman spectroscopy as shown in Figure 3a,b.[32,33] Because these single-layer thin films and the multiple-junction thin films were prepared under the same experimental conditions (the same target, pressure, laser powder, and substrate temperature), these Raman spectra also could be considered to be indirect evidence of $CaFe_2O_4$ and $ZnFe_2O_4$ compositions in the multiple junctions. Figure 4a shows *J*−*V* curves of the $CaFe_2O_4$ and $ZnFe_2O_4$ photoelectrodes. Typical photocathode and photoanode properties are observed on these two single-layer photoelectrodes, respectively. A photocathodic current, which should be due to the PEC reduction reaction, is observed on single-layer *p*-$CaFe_2O_4$ thin films, and a photoanodic current, which should be due to the PEC oxidization reaction, is observed on a single-layer *n*-$ZnFe_2O_4$ thin film. For a single-layer semiconductor electrode, whether the semiconductor acts as a photocathode or a photoanode is determined by the depletion region at the electrode−electrolyte interface (called the electrode DR). For example, in the *p*-type semiconductor electrode, the electrode DR fulfills the function of driving the electron to the surface of the photoelectrode. Thus, the *p*-type electrode is suitable as a cathode for the photoreduction. Another characteristic of the photocathode is a positive open circuit photovoltage (V_{oc}), which also results from the

dx.doi.org/10.1021/la304377z | Langmuir 2013, 29, 3116−3124

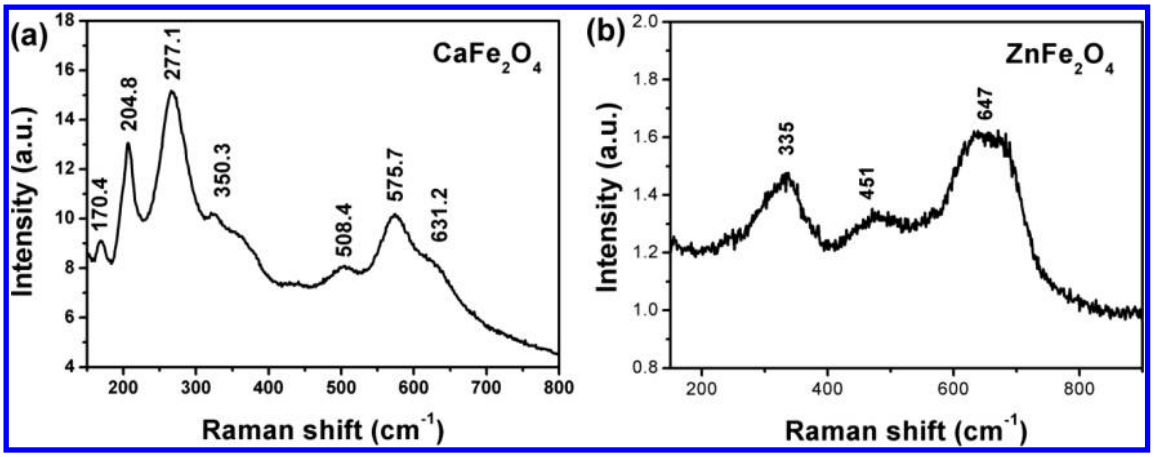

Figure 3. Raman spectra of the single-layer $CaFe_2O_4$ and $ZnFe_2O_4$ thin films.

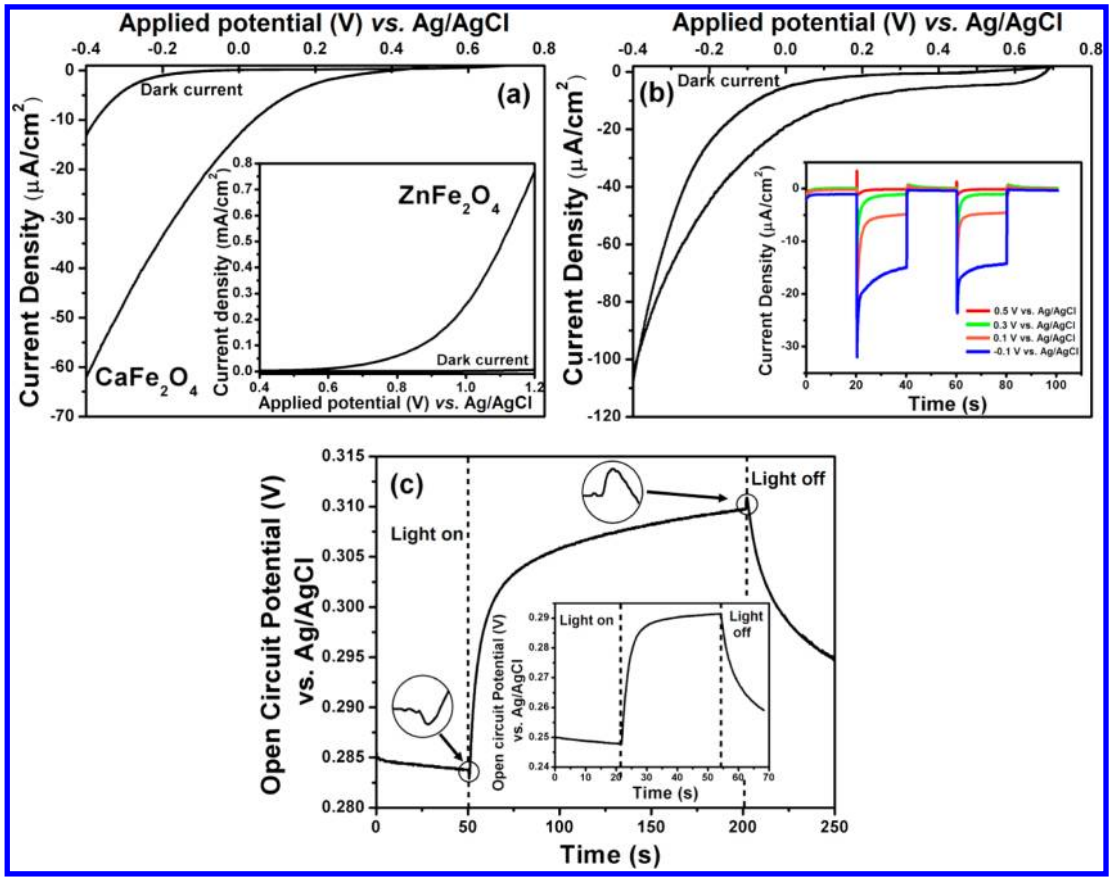

Figure 4. (a) $J-V$ graph of a single $CaFe_2O_4$ electrode, with the inset showing a $J-V$ graph of a single $ZnFe_2O_4$ electrode. (b) $J-V$ graph of a $CaFe_2O_4/ZnFe_2O_4$ *pn* junction electrode. (c) $V-t$ graph of a $CaFe_2O_4/ZnFe_2O_4$ *pn* junction electrode at 0.1 V vs Ag/AgCl, with the inset showing a $V-t$ graph of a single $CaFe_2O_4$ electrode at 0.1 V vs Ag/AgCl (430 nm monochromatic light source, 118 $\mu W/cm^2$; measured using a three-electrode configuration).

electron−hole separation caused by the electrode DR. As the inset of Figure 4c shows, under 118 $\mu W/cm^2$ of 430 nm monochromatic light, a single-layer $CaFe_2O_4$ electrode exhibits a positive V_{oc} of about 0.04 V (measured using the three-electrode configuration).

In comparison to these two single-layer electrodes, the *pn* junction ($FTO/ZnFe_2O_4/CaFe_2O_4$) photoelectrode shows a negative photocurrent and a positive photovoltage V_{oc}' (0.025 V under 430 nm monochromatic light, 118 $\mu W/cm^2$), which means that the $CaFe_2O_4/ZnFe_2O_4$ *pn* junction electrode acts as cathode with a *p*-$CaFe_2O_4$ layer as the surface contacting the electrolyte (Figure 4b,c). Different from the single-layer electrode, in the *pn* junction electrode there is another depletion region of the *pn* junction (called the junction DR), influencing the electron−hole transfer inside the photoelectrode. Therefore, the measured open circuit photovoltage V_{oc}' of the *pn* junction electrode should be equal to $V_{oc} + V_{pn}$.[33] Here, V_{oc} is the photovoltage generated by the electrode DR, and V_{pn} is the photovoltage generated by the junction DR. The $CaFe_2O_4/ZnFe_2O_4$ *pn* junction PEC cell presents positive

dx.doi.org/10.1021/la304377z | *Langmuir* 2013, 29, 3116−3124

$V_{oc}'(+)$, which is consistent with $V_{oc}(+)$ but opposite to $V_{pn}(-)$.[2,23] This implies that the electrode DR took predominance over the junction DR in the PEC performance of the *pn* junction electrode. The potential−time (V−t) graph (Figure 4c) shows that the photovoltage fluctuated in the initial seconds of light-on, also reflecting the competition between V_{oc} and V_{pn}. It is suggested that the built-in of V_{oc} is slower than that of V_{pn} after light-on (The electrode−solution system need more time to reach steady state after light irradiation in comparison to *pn* junction). At the beginning of light irradiation, the uncomplete built-in $|V_{oc}(+)|$ is smaller than $|V_{pn}(-)|$, so *pn* junction electrode presents a negative open circuit photovoltage ($V_{oc}' = V_{oc} + V_{pn} < 0$) (Figure 5a). After

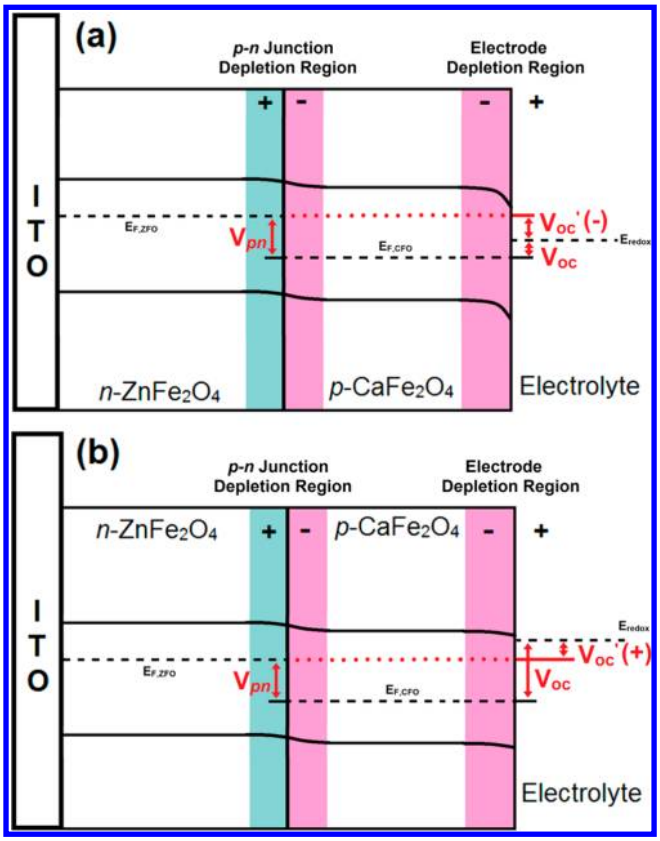

Figure 5. (a) Band structure of $CaFe_2O_4/ZnFe_2O_4$ junction at the sudden of the light irradiation. (b) Band structure of $CaFe_2O_4/ZnFe_2O_4$ junction under the light irradiation after getting stable.

V_{oc} is built-in completely, $|V_{oc}(+)|$ becomes larger than $|V_{pn}(-)|$. Thus *pn* junction electrode presents a positive open circuit photovoltage ($V_{oc}' = V_{oc} + V_{pn} > 0$) (Figure 5b). The open circuit photovoltage results also reflect the important effect of electrode DR in the performance of the *pn* junction photoelectrode. In conventional light-irradiated *pn* junction, electron only could travel from *p*-layer to *n*-layer under the force of V_{pn}. However, in *pn* junction photoelectrode PEC cell, $V_{oc}(+)$ generated by electrode DR applies across the *pn* junction as the bias. This large $V_{oc}(+)$ could neutralize $V_{pn}(-)$ and further narrow the depletion region of *pn* junction. Thus, with the assistance of $V_{oc}(+)$, the electron in *n*-$ZnFe_2O_4$ layer could diffuse to *p*-$CaFe_2O_4$ layer across the narrowed depletion region of *pn* junction. Thus, a negative photocurrent is generated in *pn* junction photoelectrode based PEC cell. Based on the results above, we clarify the function of single $CaFe_2O_4/ZnFe_2O_4$ *pn* junction photoelectrodes in a PEC cell. It is suggested that the performance of *pn* junction electrode should be determined by electrode DR and junction DR jointly. While the effect of electrode DR is stronger than junction DR, the *pn* junction with *p*-layer as the surface acts as photocathode (such as this $CaFe_2O_4/ZnFe_2O_4$ *pn* junction photoelectrode). Oppositely, while the effect of junction DR is stronger than electrode DR, the *pn* junction photoelectrode with *p*-layer as the surface acts as the photoanode.[34]

After understanding the performance of single *pn* junction photoelectrodes, we further studied the effect of the *pn* junction number on the PEC properties of the multiple-junction photoelectrodes. Four multiple-junction photoelectrodes with the same single-layer thickness of 10−15 nm but different *pn* junction numbers (10, 15, 20, and 25) were prepared by PLD method. The PEC properties of these four samples are showed in Figure 6c. With the increase of *pn* junction number from 10 to 20, the photocurrent density and the onset potential are improved remarkably. The 20-junction photoelectrode shows the highest photocurrent density (−25.23 $\mu A/cm^2$ at 0.2 V vs Ag/AgCl) and the most positive onset potential (1.10 V vs Ag/AgCl) in all four samples. Furthermore, the open circuit photovoltages of all four samples were measured with a two-electrode configuration. As Figure 6b shows, the open circuit photovoltage (V_{oc}) shows the same changing trend with the photocurrent result. V_{oc} increases significantly with the increase of the junction number and reaches the highest value of 0.97 V on the 20-junction photoelectrode. Figure 6a shows the V−t curves of the 20-junction photoelectrode and the single *pn* junction photoelectrode with the same total thickness. With the light on, the PEC cell of 20-layer $CaFe_2O_4/ZnFe_2O_4$ photoelectrode yielded a V_{oc} of 0.97 V; it was about 5 times higher than that of a single-layer junction photoelectrode (0.13 V). The enhancement of the photovoltage is suggested to be due to the increased *pn* junction number in the multiple-junction photoelectrodes but not to the thickened semiconductor layer thickness because the thickening of the layer thickness is reported to influence only the value of the photocurrent density but not the open circuit photovoltage and the onset potential.[29] It is suggested that the enhanced photovoltage generated by the multiple-junction photoelectrodes results in the improvement of the PEC properties. With the contribution of the self-generated photovoltage, the photocathodic current appears at a more positive potential; meanwhile, the photocurrent density is improved significantly. It is a novel result that the multiple-junction photoelectrode could generate a large open circuit photovoltage, the value of which is determined by the *pn* junction number in the multiple-junction photoelectrode. This result exhibits a new potential approach to providing a photovoltage for improving the PEC properties, besides using a specialized photovoltaic cell that need a tunnel layer to connect with the PEC semiconductor layer.

We also studied the effect of the single-layer thickness on the PEC properties of the multiple-junction photoelectrodes. Three samples with the same total thickness but different layer thicknesses were fabricated by the PLD method: a 10-junction photoelectrode with a single-layer thickness of about 10−15 nm (12.5 nm on average) [FTO/(12.5 nm $ZnFe_2O_4$/12.5 nm $CaFe_2O_4)_{10}$], a 5-junction photoelectrode with a single-layer thickness of about 25 nm [FTO/(25 nm $ZnFe_2O_4$/25 nm $CaFe_2O_4)_5$], and a single *pn* junction with single-layer thickness of about 125 nm [FTO/125 nm $ZnFe_2O_4$/125 nm $CaFe_2O_4$].

dx.doi.org/10.1021/la304377z | *Langmuir* 2013, 29, 3116−3124

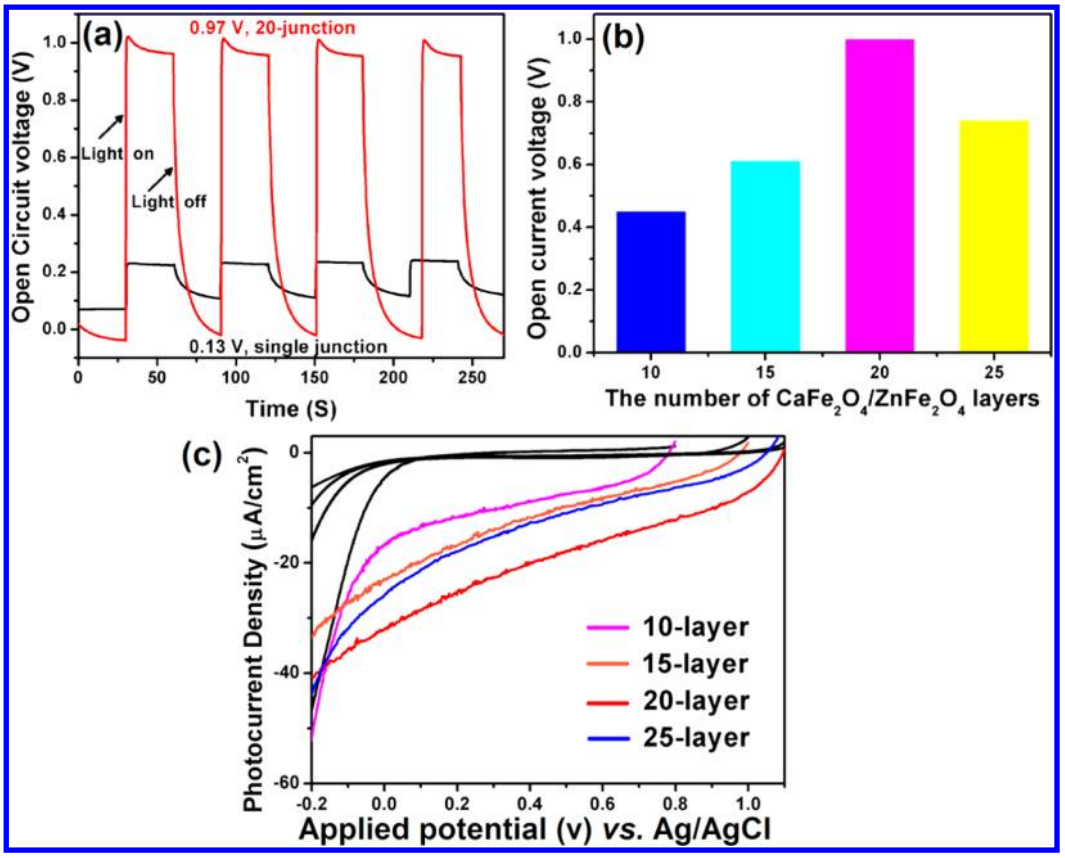

Figure 6. (a) $V-t$ curve of p-$CaFe_2O_4$/n-$ZnFe_2O_4$ junction electrode (black line) and multilayer p-$CaFe_2O_4$/n-$ZnFe_2O_4$ junction electrode (red line) under the light of a 500 W Xe lamp. (b) Open circuit photovoltage of different multilayer p-$CaFe_2O_4$/n-$ZnFe_2O_4$ junction electrodes. (c) $J-V$ curves of different multilayer p-$CaFe_2O_4$/n-$ZnFe_2O_4$ junction electrodes (0.1 M Na_2SO_4, 500 W Xe lamp).

The $J-V$ curves of these three samples are shown in Figure 7. The 5-junction and 10-junction photoelectrodes show much higher photocurrent densities than a single *pn* junction photoelectrode. The photocurrent density of the 10-junction photoelectrode is higher than that of the 5-junction photoelectrode in the region from 0.33 to 0.80 V versus Ag/AgCl but lower than that of the 5-junction photoelectrode in the region from −0.20 to 0.33 V versus Ag/AgCl. Compared to a single *pn* junction photoelectrode, the multiple-junction samples with different single-layer thicknesses both show the obvious enhancement effect on the PEC properties. Furthermore, the multiple-junction photoelectrode with a 12.5 nm single-layer thickness could efficiently enhance the photocurrent density at the relative positive potential (0.33 to 0.80 V vs Ag/AgCl). In contrast, the multiple-junction photoelectrode with a 25 nm single-layer thickness could efficiently enhance the photocurrent density in the relatively negative potential region (−0.20 to 0.33 V vs Ag/AgCl). These results indicated that the single-layer thickness greatly influences the PEC properties of the multiple-junction photoelectrodes. The multiple-junction photoelectrode with thin single-layer thickness shows an obvious negative photocurrent at a relative positive potential, reflecting the fact that the multiple-junction structure with a thin single-layer thickness is helpful in reducing the dependence of PEC properties on the applied potential.

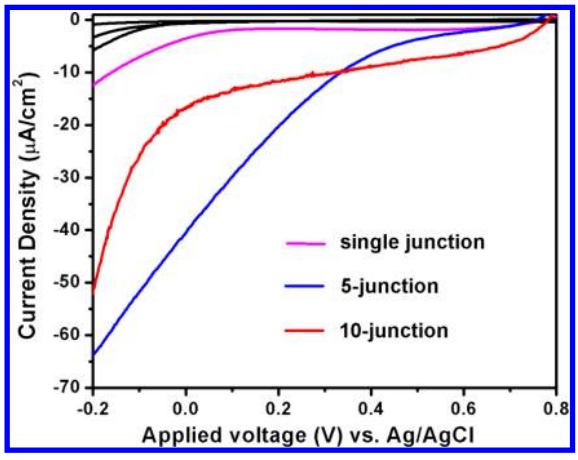

Figure 7. $J-V$ curves of three photoelectrodes (single-junction photoelectrode, 5-junction photoelectrode, and 10-junction photoelectrode) with the same total thickness but different single-layer thicknesses.

On the basis of the experimental results above, we assumed a model to depict the function of the multiple $CaFe_2O_4$/$ZnFe_2O_4$ *pn* junction photoelectrodes. Figure 8c presents the assumed schematic diagram of the multilayer $CaFe_2O_4$/$ZnFe_2O_4$ *pn* junction photoelectrode, which is treated as a series of interconnected *pnp* junctions. The calculated thickness of the electrode DR at the $CaFe_2O_4$-layer-electrolyte interface was about 2.8 nm (calculation process in the Supporting Information). Therefore, it is rational that the electrode DR is located only in the outmost $CaFe_2O_4$ layer and fulfills its function of separating an electron and a hole completely even when the single-layer thickness was decreased to the 10 nm scale. Because the thickness of single layer is only 10−15 nm,

dx.doi.org/10.1021/la304377z | *Langmuir* 2013, 29, 3116−3124

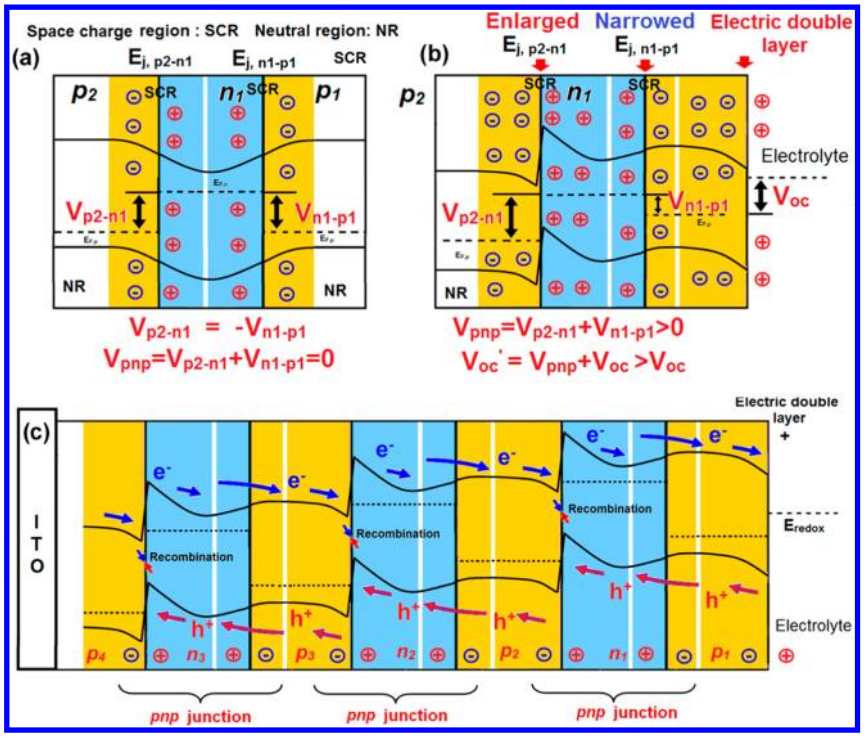

Figure 8. (a) Schematic of a single *pnp* junction under light irradiation. (b) Schematic of a *pnp* junction electrode in the electrolyte under light irradiation. (c) Schematic of a multilayer *pnp* junction electrode in the electrolyte under light irradiation.

the neutral region is quite small and the depletion region fill most of the region of the multiple *pn* junction. First, we focus on the outermost p_2-n_1-p_1 junction, of which p_1 contacts the electrolyte. For a conventional *pnp* junction under light irradiation without contacting the electrolyte, symmetrical space charge fields $E_{j,p_2\text{-}n_1}$ and $E_{j,n_1\text{-}p_1}$ ($E_{j,p_2\text{-}n_1} = -E_{j,n_1\text{-}p_1}$) should generate two photovoltages with the same amplitude in opposite directions ($V_{p_2\text{-}n_1} = -V_{n_1\text{-}p_1}$), as shown in Figure 8a. Thus, the total photovoltage (V_{pnp}) of *pnp* junction should be zero. While the *pnp* junction is set as the electrode, the electrode DR generates an additional positive photovoltage as the bias on the *pnp* junction (Figure 8b). The positive photovoltage (V_{oc}) was in agreement with $E_{j,p_2\text{-}n_1}$ but in conflicting with $E_{j,n_1\text{-}p_1}$. Thus, $E_{j,p_2\text{-}n_1}$ was strengthened while $E_{j,n_1\text{-}p_1}$ was weakened.[35] As a result, $E_{j,p_2\text{-}n_1}$ yielded a positive photovoltage ($V_{p_2\text{-}n_1}$) with a larger amplitude than that of the negative photovoltage ($V_{n_1\text{-}p_1}$) yielded by $E_{j,n_1\text{-}p_1}$. This indicates that $V_{pn\text{-}p} = V_{p_2\text{-}n_1} + V_{n_1\text{-}p_1} > 0$ and that the total photovoltage ($V_{p_2\text{-}n_1\text{-}p_1\text{-solution}}$) of the p_2-n_1-p_1-solution system is greater than V_{oc} because of $V_{p_2\text{-}n_1\text{-}p_1\text{-solution}} = V_{pn\text{-}p} + V_{oc} > V_{oc}$.

As to the next p_3-n_2-p_2 junction on which a positive $V_{p_2\text{-}n_1\text{-}p_1\text{-solution}}$ is applied, similar reasoning leads to such a conclusion that $V_{p_3\text{-}n_2\text{-}p_2\text{-}n_1\text{-}p_1\text{-solution}} > V_{p_2\text{-}n_1\text{-}p_1\text{-solution}}$. Accordingly, the rest may be deduced by analogy. If we assume that N is the layer number, then $V_{p_N\text{-}\cdots\text{-}p_1\text{-solution}} > \ldots > V_{p_2\text{-}n_1\text{-}p_1\text{-solution}}$. This model could explain the phenomenon that the open circuit photovoltage increases gradually with the increase in the *pn* junction number in a photoelectrode. However, it should be noticed that the photovoltage generated by each *pnp* junction is greatly influenced by the intensity of absorbed light. The increase in the *pn* junction number indicates that the inner *pnp* junctions could absorb very little light and could not supply the resulting photovoltage. In the competition between the multiple-junction enhancement effect and the limitation of light absorption, the 20-layer $CaFe_2O_4/ZnFe_2O_4$ heterojunction has the best PEC properties.

Another important issue is the transfer of a photogenerated carrier in the multiple $CaFe_2O_4$/ $ZnFe_2O_4$ *pn* junction. As illustrated in Figure 8c, under the force of the photovoltage V_{oc} and the applied potential, the holes transfer from p_1 to n_1 through the narrowed p_1-n_1 depletion region. Then, the holes diffuse across the neutral region of n_1 within their lifetime because the single-layer thickness was as small as around several dozen nanometers. After the depletion region between n_1 and p_2 is entered, under the force of the enlarged space charge field the holes move to the interface of n_1 and p_2, where the holes recombine completely with the electrons from p_2. By parity of reasoning, the following *pnp* junctions repeated analogous carrier transportation. This assumed carrier transfer route could explain the effects of the different single-layer thicknesses on the PEC properties. The depletion region of a *pn* junction usually has a fixed thickness depending on the materials in the *pn* junction, so the increase in the single-layer thickness directly enlarges the area of the neutral region. In the sample with a thick single-layer thickness, the neutral region is still large so that most of the carriers do not easily diffuse across the neutral region of the *n* layer in their lifetime. Enhancing the applied potential (in the negative direction) could widen the depletion region between n_1 and p_2 and thus narrow the neutral region, so the photocurrent density increases drastically from 0 as the applied potential becomes negative gradually. For the sample with a thin single-layer thickness, the neutral region of the junction is thinner so that most of the carriers could transfer through the neutral region even at a relative positive applied potential, so the multiple-junction photoelectrode with thin single-layer thickness exhibits an obvious photocurrent at a

dx.doi.org/10.1021/la304377z | *Langmuir* 2013, 29, 3116−3124

relative positive applied potential. However, it should be noticed that the photocurrent density of the multiple-junction photoelectrode should be determined by the photocurrent density generated by the single *pnp* junction because the carrier of a single *pnp* junction could recombine only with the carrier from the neighboring *pnp* junction. The photocurrent density of a single *pnp* junction is strongly determined by the intensity of absorbed light, which is directly influenced by the single-layer thickness. With this limitation, the photocurrent density of the multiple-junction photoelectrode with a thin single-layer thickness did not show a remarkable improvement when the applied potential became much more negative.

From the results above, it is clarified that the multiple-junction structure is favorable for improving the PEC properties of the photoelectrodes. The increase in the junction number in a multiple-junction photoelectrode enhances the open circuit photovoltage remarkably. The nanomultiple-junction structure in the photoelectrode favors the carrier transfer and reduces the dependence of PEC properties on the applied voltage. With the joint effect of these two advantages, the multiple-junction photoelectrode exhibits wonderful PEC properties (a high photocurrent density and a favorable onset potential). Our results provide a potential approach to reducing the dependence of the PEC properties on the applied potential. It should be helpful in improving the efficiency of PEC water splitting further.

CONCLUSIONS

Multiple $CaFe_2O_4$/ $ZnFe_2O_4$ *pn* junction thin films were prepared successfully by the PLD method. These multiple-junction photoelectrodes had an obvious enhancement effect on the PEC properties, including the photocurrent density and the onset potential. The multiple $CaFe_2O_4$/ $ZnFe_2O_4$ *pn* junction photoelectrodes also yielded a high open circuit photovoltage up to 0.97 V. It is found that the multiple-junction structure could enhance the open circuit photovoltage efficiently and improve the carrier transfer inside the photoelectrodes. Our results provide a novel approach to reducing the dependence of PEC properties on the applied potential and also raising the possibility of utilizing the multiple-junction structure to improve the PEC properties of the photoelectrodes. With regard to the deficiency that the photocurrent density of the multiple-junction photoelectrode is greatly limited by the photocurrent density of a single *pnp* junction, it may be solved by selecting a semiconductor with a much longer diffusion length (such as TiO_2) to prepare the multiple-junction photoelectrodes. The further study following this idea is ongoing.

ASSOCIATED CONTENT

Supporting Information

Information for the *p*-$CaFe_2O_4$/*n*-$ZnFe_2O_4$ photoelectrode. This material is available free of charge via the Internet at http://pubs.acs.org.

AUTHOR INFORMATION

Corresponding Author

*Tel: +81-029-859-2646. E-mail: jinhua.ye@nims.go.jp.

Present Addresses

[⊥]School of Chemistry and Chemical Engineering, Southeast University, Nanjing 211189, P. R. China.

[#]State Key Laboratory for Oxo Synthesis & Selective Oxidation and National Engineering Research Center for Fine Petrochemical Intermediates, Lanzhou Institute of Chemical Physics, Lanzhou, P.R. China.

Notes

The authors declare no competing financial interest.

ACKNOWLEDGMENTS

This work was partially supported by the World Premier International Research Center Initiative on Materials Nanoarchitectonics, MEXT, Japan.

REFERENCES

(1) Fujishima, A.; Honda, K. Electrochemical Photolysis of Water at a Semiconductor Electrode. *Nature* **1972**, *238*, 37−38.

(2) Walter, M. G.; Warren, E. L.; McKone, J. R.; Boettcher, S. W.; Mi, Q. X.; Santori, E. A.; Lewis, N. S. Solar Water Splitting Cells. *Chem. Rev.* **2010**, *110*, 6446−6473.

(3) Hoffmann, M. R.; Martin, S. T.; Choi, W.; Bahnemann, D. W. Environmental Applications of Semiconductor Photocatalysis. *Chem. Rev.* **1995**, *95*, 69−96.

(4) Ida, S.; Matsumoto, Y.; Ishihara, T. Preparation of p-Type $CaFe_2O_4$ Photocathodes for Producing Hydrogen from Water. *J. Am. Chem. Soc.* **2010**, *132*, 17343−17345.

(5) Kay, A.; Cesar, I.; Gratzel, M. New Benchmark for Water Photooxidation by Nanostructured α-Fe_2O_3 Films. *J. Am. Chem. Soc.* **2006**, *128*, 15714−15721.

(6) Sivula, K.; Formal, F. L.; Gratzel, M. WO_3−Fe_2O_3 Photoanodes for Water Splitting: A Host Scaffold, Guest Absorber Approach. *J. Chem. Mater.* **2009**, *21*, 2862−2867.

(7) Vinodgopal, K.; Bedja, I.; Kamat, P. V. Article Nanostructured Semiconductor Films for Photocatalysis. Photoelectrochemical Behavior of SnO_2/TiO_2 Composite Systems and Its Role in Photocatalytic Degradation of a Textile Azo Dye. *Chem. Mater.* **1996**, *8*, 2180−2187.

(8) Nozik, A. J. *p-n* Photoelectrolysis Cells. *Appl. Phys. Lett.* **1976**, *29*, 150−153.

(9) Miller, E. L.; Rocheleau, R. E.; Deng, X. M. Design Considerations for a Hybrid Amorphous Silicon/Photoelectrochemical Multijunction Cell for Hydrogen Production. *Int. J. Hydrogen Energy* **2003**, *28*, 615−623.

(10) Mor, G. K.; Varghese, O. K.; Grimes, C. A. Enhanced Photocleavage of Water Using Titania Nanotube Arrays. *Nano Lett.* **2005**, *5*, 191−195.

(11) Paulose, M.; Shankar, K.; Grimes, C. A. Anodic Growth of Highly Ordered TiO_2 Nanotube Arrays to 134 μm in Length. *J. Phys. Chem. B.* **2006**, *110*, 16179−16184.

(12) Aroutiounian, V. M.; Arakelyan, V. M.; Shahnazaryan, G. E. Metal Oxide Photoelectrodes for Hydrogen Generation Using Solar Radiation-Driven Water Splitting. *Sol. Energy* **2005**, *78*, 581−592.

(13) Torres, G. R.; Lindgren, T.; Lindquist, S. E. Photoelectrochemical Study of Nitrogen-Doped Titanium Dioxide for Water Oxidation. *J. Phys. Chem. B.* **2004**, *108*, 5995−6003.

(14) Wang, H.; Lindgren, T.; Lindquist, S. E. Photolelectrochemistry of Nanostructured WO_3 Thin Film Electrodes for Water Oxidation: Mechanism of Electron Transport. *J. Phys. Chem. B.* **2000**, *104*, 5686−5696.

(15) Khan, S. U. M.; Ingler, W. B., Jr. Efficient Photochemical Water Splitting by a Chemically Modified n-TiO_2. *Science* **2002**, *297*, 2243−2245.

(16) Heller, A.; Vadimsky, R. G. Efficient Solar to Chemical Conversion: 12% Efficient Photoassisted Electrolysis in the [p-type InP(Ru)]/HCl-KCl/Pt(Rh) Cel. *Phys. Rev. Lett.* **1981**, *46*, 1153−1156.

(17) Li, C.; Wang, F.; Yu, J. C. Semiconductor/Biomolecular Composites for Solar Energy Applications. *Energy Environ. Sci.* **2011**, *4*, 100−113.

(18) Wang, X.; Zhu, H.; Xu, Y.; Wang, H.; Tao, Y.; Hark, S.; Xiao, X.; Li, Q. Aligned ZnO/CdTe Core−Shell Nanocable Arrays on Indium

Tin Oxide: Synthesis and Photoelectrochemical Properties. *ACS Nano* **2010**, *4*, 3302−3308.
(19) Myung, Y.; Jang, D. M.; Park, J. Crystallinity Dependence of the Plasmon Resonant Raman Scattering by Anisotropic Gold Nanocrystals. *ACS Nano* **2010**, *4*, 3789−3800.
(20) Hartmann, P.; Lee, D.; Smarly, B.; Janek, J. Mesoporous TiO_2: Comparison of Classical Sol−Gel and Nanoparticle Based Photoelectrodes for the Water Splitting Reaction. *ACS Nano* **2010**, *4*, 3147−3154.
(21) Chen, X.; Ye, J.; Ouyang, S. Enhanced Incident Photon-to-Electron Conversion Efficiency of Tungsten Trioxide Photoanodes Based on 3D-Photonic Crystal Design. *ACS Nano* **2011**, *5*, 4310−4318.
(22) Itoh, K.; Bockris, J. O'M. Stacked Thin-Film Photoelectrode Using Iron Oxide. *J. Appl. Phys.* **1984**, *56*, 874−876.
(23) Liou, F. T.; Yang, C. Y. P. Photoelectrolysis at Fe_2O_3/TiO_2 Heterojunction Electrode. *J. Electrochem. Soc.* **1982**, *129*, 342−345.
(24) Liu, D.; Kamat, P. V. Photoelectrochemical Behavior of Thin Cadmium Selenide and Coupled Titania/Cadmium Selenide Semiconductor Films. *J. Phys. Chem.* **1993**, *97*, 10769−10773.
(25) Khaselev, O.; Turner, J. A. A Monolithic Photovoltaic-Photoelectrochemical Device for Hydrogen Production via Water Splitting. *Science* **1998**, *280*, 425−427.
(26) Khaselev, O.; Turner, J. A. High-efficiency Integrated Multijunction Photovoltaic/Electrolysis Systems for Hydrogen Production. *Int. J. Hydrogen Energy* **2001**, *26*, 127−132.
(27) Gratzel, M. Photoelectrochemical Cells. *Nature* **2001**, *414*, 338−344.
(28) Hook, J. R. Hall, H. E. *Solid State Physics*, 2nd ed.; Wiley, 1991.
(29) Matsumoto, Y.; Omae, M.; Sato, E. New Photocathode Materials for Hydrogen Evolution: $CaFe_2O_4$ and $Sr_7Fe_{10}O_{22}$. *J. Phys. Chem.* **1987**, *91*, 577−581.
(30) Matsumoto, Y. Energy Positions of Oxide Semiconductors and Photocatalysis with Iron Complex Oxides. *J. Solid State Chem.* **1996**, *126*, 227−234.
(31) Kim, H. G.; Borse, P. H.; Jang, J. S.; Jeong, E. D.; Jung, O.-S.; Suh, Y. J.; Lee, J. S. Fabrication of $CaFe_2O_4/MgFe_2O_4$ Bulk Heterojunction for Enhanced Visible Light Photocatalysis. *Chem. Commun.* **2009**, 5889−5891.
(32) Romcevic, N.; Sibera, D. Raman Scattering from ZnO(Fe) Nanoparticles. *Acta Phys. Pol., A* **2008**, *114*, 1323−1328.
(33) Cao, J.; Kako, T.; Ye. Fabrication of *p*-type $CaFe_2O_4$ Nanofilms for Photoelectrochemical Hydrogen Generation. *J. Electrochem. Commun.* **2011**, *13*, 275−278.
(34) Lin, Y.; Xu, Y.; Wang, D. Growth of p-Type Hematite by Atomic Layer Deposition and Its Utilization for Improved Solar Water Splitting. *J. Am. Chem. Soc.* **2012**, *134*, 5508−5511.
(35) Dalven, R. *Introduction to Applied Solid State Physics*; Plenum Press: New York, 1980.